46th AIAA/ASME/SAE/ASEE Joint Propulsion Conference & Exhibit
25 - 28 July 2010, Nashville, TN

AIAA 2010-7103

Ion Velocity Distribution in a Low-Power Cylindrical Hall Thruster

Natalia A. MacDonald and Mark A. Cappelli
Stanford Plasma Physics Laboratory
Stanford University
Stanford, CA 94305

William A. Hargus, Jr.
Spacecraft Propulsion Branch
Air Force Research Laboratory
Edwards AFB, CA 93524

This work presents time-averaged ion velocity and energy distributions in the axial direction within the acceleration channel and axial and radial directions in the plume of a Princeton University low power cylindrical Hall thruster operating on xenon. Xenon ion velocities for the thruster are derived from laser-induced fluorescence measurements of the $5d[4]_{7/2} - 6p[3]_{5/2}$ xenon ion excited state transition at $\lambda = 843.72$ nm. Two operating conditions are considered with variations to the magnetic field strength, in an effort to capture the effect on ion velocity distributions. The lower magnetic field condition is also considered with a higher vacuum chamber background pressure. Under nominal conditions, xenon ions are accelerated to a most probable energy of 25 eV within the thruster with an additional 175 eV gain in the thruster plume. At a position 40 mm into the plume, this constitutes an energy of 200 eV, with the wings of the energy distribution extending between 177 and 228 eV at an applied potential of 300 V.

I. Introduction

This study characterizes time-averaged xenon ion velocity and energy distributions both inside the acceleration channel and in the near field plume of a low power cylindrical Hall thruster (CHT) using laser-induced fluorescence (LIF). It is a continuation of a previous study in which the most probable axial, radial and azimuthal velocities within the acceleration channel and in the plume of a low power cylindrical Hall thruster were reported.[1] LIF measurements are also used to assess the effect of varying magnetic field strength on the evolution of the ion velocity and kinetic energy profiles.

The thruster used in this study is the Princeton University CHT-30. Previous efforts examining low power annular Hall effect thrusters have shown that erosion of the insulator protecting the central magnetic pole limits thruster lifetime significantly, even more so than erosion of the outer insulator. This effect is amplified as the power and size of the Hall thruster is scaled down. By reducing the length of the central magnetic pole and creating a region of the channel with a low surface-to-volume area (a cylindrical region), the CHT as developed by Princeton University reduces the impact of insulator erosion significantly.[2]

The CHT-30 has a cylindrical acceleration channel with a diameter of 30 mm and depth of 13 mm. This is similar to most modern Hall thrusters, which have acceleration channels with a maximum depth of 10-20 mm. With this geometry, it is possible to align collection optics to the probe beam such that limited internal optical access is possible without thruster modification. In this work, the collection lens is placed 60° off the plume axis.[3] With the CHT's plume divergence half angle of approximately 60° to 80°,[4] this places the collection optics away from much of the plume ion flux. In this way, it is possible to probe internal

ion acceleration of the CHT-30 with minimal intrusion into the plume and without distroying the collection optics through sputtering.

Two thruster operating conditions are examined in this study. These include an nominal condition for which there is unpublished performance data, and an reduced magnetic field condition. The goals of these measurements are to characterize the ion velocity for a known case, and examine a low plasma oscillation case where the signal-to-noise ratio (SNR) of the diagnostic is maximized.

II. Experimental Apparatus

A. Xenon Ion Spectroscopy

For the results reported here, the $5d[4]_{7/2}-6p[3]_{5/2}$ electronic transition of Xe II at 834.72 nm is probed. The isotopic and nuclear-spin effects contributing to the hyperfine structure of the $5d[4]_{7/2}-6p[3]_{5/2}$ xenon ion transition produce a total of 19 isotopic and spin split components. The hyperfine splitting constants which characterize the variations in state energies are only known for a limited set of energy levels. Unfortunately, this xenon ion transition only has confirmed data on the nuclear spin splitting constants of the $6p[3]_{5/2}$ upper state.[5–8]

Manzella first used the $5d[4]_{7/2}-6p[3]_{5/2}$ xenon ion transition at 834.72 nm to make velocity measurements in a Hall thruster plume.[9] A convenient feature of this transition is the presence of a relatively strong line originating from the same upper state ($6s[2]_{3/2}-6p[3]_{5/2}$ transition at 541.9 nm,[10] which allows for non-resonant fluorescence collection). Ion velocity is simply determined by measurement of the Doppler shift of the absorbing ions.[11]

B. Test Facility

The LIF measurements were performed in Chamber 6 of the Air Force Research Laboratory (AFRL) Electric Propulsion Laboratory at Edwards AFB, CA. This experimental apparatus has been described extensively in previous work.[1,3,12] Chamber 6 is a non-magnetic stainless steel chamber with a 1.8 m diameter and 3 m length. It has a measured pumping speed of 32,000 L/s on xenon. Pumping is provided by four single stage cryogenic panels (single stage cold heads at 25 K) and one 50 cm two stage cryogenic pump (12 K). Chamber pressure during thruster operation is approximately 2.8×10^{-6} torr, corrected for xenon.

Figure 1 shows a top view of the laser optical train, collection optics, and one leg of the external probe optics. The laser is a tunable diode laser, capable of tuning approximately ±50 GHz about a center wavelength of 834.72 nm. The laser beam passes through several beam pick-offs followed by a 50-50 cube beam splitter where it is split into two beams of equal power, approximately 5 mW each. The first beam, the axial probe beam shown in Figures 1 and 2 is focused by a lens and enters the vacuum chamber through a window. A second probe beam, shown in Figure 2 only, is directed from the optical bench via a periscope apparatus so that it enters the chamber from above the thruster and probes the velocity perpendicular to the first probe beam. Each probe beam is chopped at a unique frequency by choppers Ch2 (2kHz) and Ch3 (2.8 kHz) for phase sensitive detection of the fluorescence signals.

The two wedge beam pick-offs (BS) shown in Figure 1 provide portions of the beam for diagnostic purposes. These diagnostics include a commercial wavelength meter and a 300 MHz free spectral range Fabry-Perot etalon (F-P) to monitor wavelength during a laser scan, and a low pressure xenon hollow cathode discharge lamp to provide a stationary absorption reference for the determination of the Doppler shift. Unfortunately, there is no detectable population of the ionic xenon $5d[4]_{7/2}$ state. However, there is a nearby (estimated to be 18.1 GHz distant) neutral xenon $6s'[1/2]_1-6p'[3/2]_2$ transition at 834.68 nm.[13,14]

The fluorescence collection optics are also shown in Figure 1. The fluorescence is collected by a 75 mm diameter, 300 mm focal length lens within the chamber and oriented 60° from the probe beam axis. The collimated fluorescence signal is directed through a window in the chamber side wall to a similar lens that focuses the collected fluorescence onto the entrance slit of the 125 mm focal length monochrometer with a photomultiplier tube (PMT). Due to the 1:1 magnification of the collection optics, the spatial resolution of the measurements is determined by the geometry of the entrance slit 0.7 mm width and 1.5 mm height as well as the sub-mm diameter of the probe beam. This apparatus allows for limited probing of the interior acceleration channel of Hall thrusters with relatively shallow acceleration channels. Measurements suggest

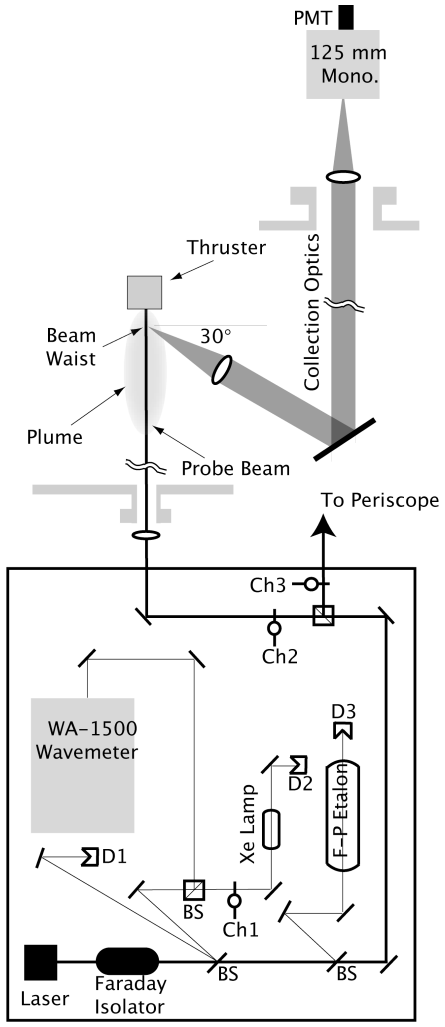

Figure 1. Top view diagram of the laser optical train and collection optics. Note that the radial probe beam periscope and focusing optics are not shown.

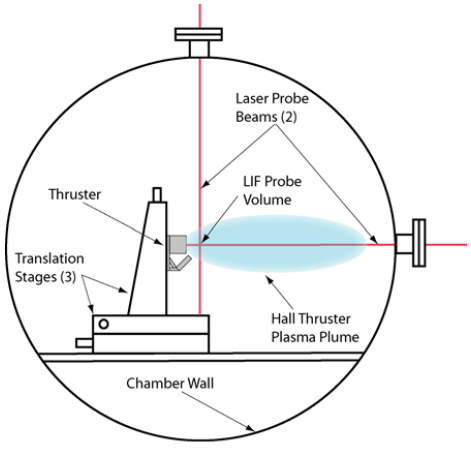

Figure 2. Side view diagram of thruster within AFRL chamber 6. Also shown are the translation stages and the laser probe beams. Note that the fluorescence collection and external optics are not shown.

that this combination of apparatus and laser power are well within the linear fluorescence regime.

The uncertainty of the velocity measurements is estimated to be within ±500 m/s for the most probable values. The repeatability of the peak locations appear to be a fraction of the quoted uncertainty. However, the fluorescence line shapes are often significantly broadened, presumably due to wide velocity distributions caused by plasma fluctuations. The quoted uncertainty should therefore be viewed as the uncertainty in the determination of the peak of the fluorescence line shape.

C. Cylindrical Hall Thruster

The thruster used in this study is the CHT-30 cylindrical Hall thruster developed by Princeton University. The CHT-30 has a 30 mm diameter channel that is composed of a short annular region near the anode followed by a 13 mm long cylindrical region as shown in Figure 3.[15] This figure also indicates the magnetic field topology seen during the operation of the thruster. CHTs have been of interest in the electric propulsion community in recent years due to their low power operation and potential for long life. The low surface-to-volume ratio of their acceleration channel and cusped magnetic field configuration result in low erosion rates of their ceramic wall materials, which is especially desirable when scaling down in power. CHTs have also demonstrated performance levels approaching those of state-of-the-art annular Hall thrusters.[2]

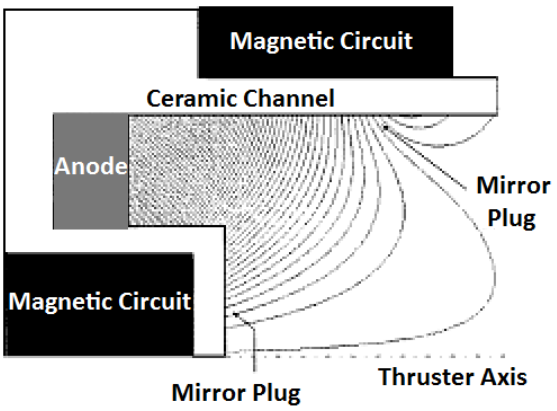

Figure 3. CHT Magnetic field distribution for cusped field configuration.[15]

Although the CHT and several other magnetic cusp electrostatic thrusters have elements that superficially resemble Hall effect thrusters, this thruster type has several features that make it considerably different.[16] First, the high magnetic field strengths within cusp thrusters suggest that the ions may be magnetized. Ion magnetization is understood not to exist in annular Hall thrusters. Furthermore, the geometry and magnetic field structure of cusp thrusters are notably different, with the cusped magnetic field shape seeing no analog in traditional Hall thrusters. In this early stage of research, these differences appear to indicate that the electron transport mechanism within cusp thrusters also differs significantly. The azimuthal $\vec{E} \times \vec{B}$ drift seen in conventional Hall thrusters is either lacking or occurs very near the anode of the cusp thruster. This suggests that the $E \times B$ shear that appears critical in annular Hall thruster electron transport does not exist, or assumes a very different form in cusp thrusters.[1,2]

D. Operating Conditions

The operating conditions considered in this study were a nominal operating condition provided in Table 1, as well as an reduced magnetic field condition provided in Table 2. The reduced magnetic field operating condition was chosen due to the quiescent operating mode of the thruster and the improved fluorescence signal quality throughout the majority of the plume. It also gave insight into the influence of the magnetic field strength on the ion velocity profiles. These conditions were run with a chamber background pressure of 2.8×10^{-6} torr, corrected for xenon. The reduced magnetic field condition was also run at a higher chamber background pressure of 3.5×10^{-5} torr to examine the effect of varying the vacuum chamber conditions.

Table 1. Nominal CHT-30 operating conditions.

Anode Flow	390 μg/s Xe
Cathode Flow	98 μg/s Xe
Anode Potential	300 V
Anode Current	0.53 A
Keeper Current	OFF
Heater Current	5.0 A
Magnet 1 Current	3.00 A
Magnet 2 Current	2.00 A

Table 2. Reduced Magnetic Field CHT-30 operating conditions.

Anode Flow	390 μg/s Xe
Cathode Flow	150 μg/s Xe
Anode Potential	300 V
Anode Current	0.61 A
Keeper Current	0.30 A
Heater Current	5.0 A
Magnet 1 Current	2.00 A
Magnet 2 Current	2.00 A

Figure 4 depicts the Cartesian coordinate system used in these measurements. Figure 5 shows a side view of the thruster channel and plume including the positions of the LIF data points examined in this paper. The thruster is mounted on a three axes orthogonal computer controlled translation system which allows for precise motion in the X-, Y- and Z-axes. Measurements at various Y-positions provided radial and axial data. In this paper, ion velocity and subsequently derived kinetic energy distributions are presented along the centerline of the thruster axis at positions from $Z = -6$ mm to +40 mm into the plume. The depth at which the data points could be collected inside the thruster channel was limited by the angle inside the thruster visible to the collection optics (60° from the leading edge of the channel). Additionally, distributions are presented along the exit plane of the thruster at $Z = 0$ mm with a 2 mm spatial resolution in the Y-direction from $Y = 0$ mm to +14 mm.

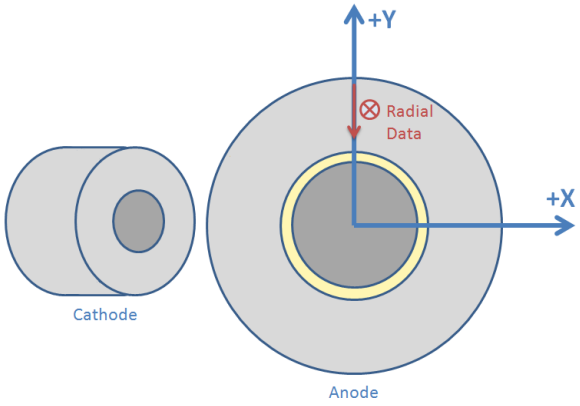

Figure 4. Coordinate system used for data points.

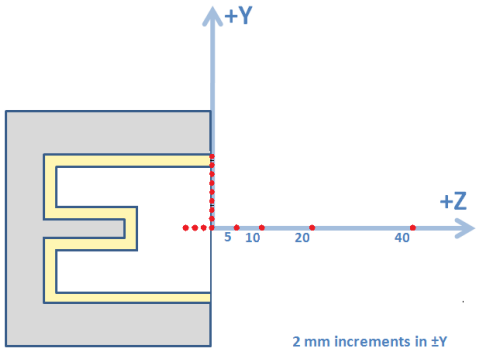

Figure 5. Location of data points for axial and radial LIF measurements.

III. Results and Discussion

Two operating conditions are presented in this study of the ion velocity and energy distributions of the CHT-30: a nominal operating condition and a condition with reduced magnetic field strength. The reduced magnetic field condition has approximately 70% of the magnetic field strength, and provides a quiescent operating mode of the thruster. Comparisons are made between these two conditions for positions along the centerline and across the exit plane of the thruster. Additionally, the reduced magnetic field case was run at high vacuum chamber background pressure. Comparisons between this high pressure condition and the nominal operating condition are made along the centerline of the thruster. The velocity and energy distributions are each area-normalized.

A. Lineshape Analysis

Analysis of the fluorescence measurements made on the CHT-30 provides a great deal of information about the motion of the ions both in the channel and in the plume of the thruster. A raw LIF signal is a convolution of the ion velocity distribution function (VDF), and the transition lineshape (including broadening effects due to instruments, the finite linewidth of the laser, etc.). The transition lineshape is typically much narrower than the VDF,[17] and therefore the velocity distribution can often be represented directly by the raw LIF trace.[18] It has previously been shown that the difference between a deconvolved VDF and the raw LIF signal is small, less than 20% – in some cases, such as VDFs with low SNR and broad velocity distributions, it can even be advantageous to forgo deconvolution due to the additional oscillatory noise it often produces near trace end points.[19] Therefore, the ion velocity distributions presented in this paper are given by the raw fluorescence traces.

Figures 6 and 7 show the analysis process for a fluorescence measurement taken at $Y = 0$ mm and $Z = 20$ mm. Figure 6 shows the raw absorption and LIF traces in relative frequency units. The Doppler shift relationship is used between the stationary absorption reference and the LIF traces to transform the frequency separation into velocity units, as shown in Figure 7. In this figure, the blue curve represents the axial VDF, while the black curve is the axial kinetic energy distribution. When normalized such that the total area under the curve is equal to unity, these traces represent the probability of an ion having a given velocity or kinetic energy at that spatial point. The kinetic energy is derived using a simple $\frac{1}{2}m_i v^2$ relationship to the VDF, where m_i is the mass of the xenon ion.

In Figure 7, both the velocity and kinetic energy curves are normalized such that the peak is at a value of 1 (rather than area normalized). This is useful in determining the median values of velocity and kinetic energy. The green and red curves represent the integral of the velocity and kinetic energy curves, respectively. The point where these integrated lines crosses 0.5 indicates the median value on their corresponding velocity or kinetic energy distribution. At $Y = 0$ mm and $Z = 20$ mm, the median velocity is 14,000 m/s, and the median kinetic energy is 138 eV.

To capture the range of velocities or energies over which the majority of ions are moving, it is possible to see where the integral curves meet a certain percentage above and below the 50% mark. For one standard

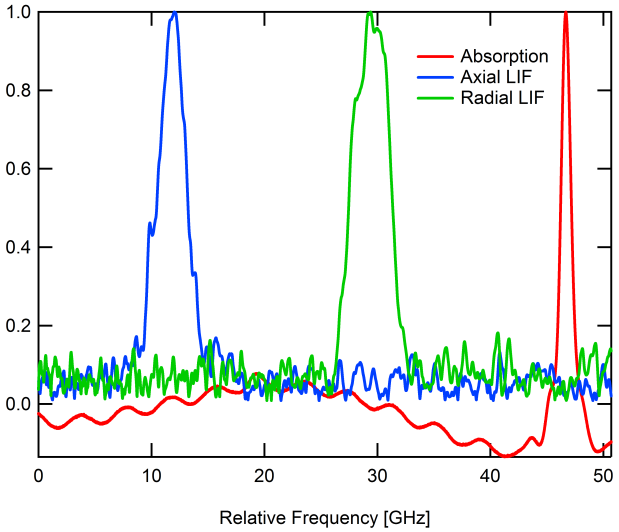

Figure 6. Example of LIF and absorption traces taken at Y = 0 mm and Z = 20 mm.

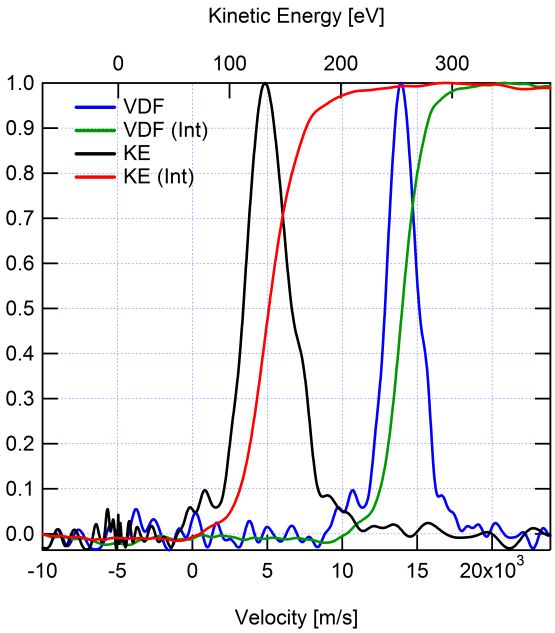

Figure 7. Lineshape analysis for axial ion velocity and kinetic energy distributions at Y = 0 mm, Z = 20 mm. VDF represents the velocity distribution function, KE represents the kinetic energy distribution function, and Int represents the integral of each function.

deviation above and below the median value, approximately 68% of the ions have axial velocities between 12,700 m/s and 15,200 m/s (115 eV to 161 eV). Similarly, for two standard deviations, approximately 95% of the ions have an axial velocity between 10,600 m/s and 17,200 m/s (84.3 eV to 210 eV).

In most cases the median values are very close to the mean values, due to the symmetry of the distributions (i.e. at $Y = 0$ mm and $Z = 20$ mm, the mean velocity is 13,900 m/s and mean kinetic energy is 138 eV, the most probable velocity is 14,500 m/s and most probable kinetic energy is 143 eV). For a pure gaussian distribution, the mean, median and most probable (or peak) values are by definition identical. However, the oscillatory nature of these thrusters along with low fluorescence signal strength cause the fluorescence traces to have low SNR, mostly due to the baseline noise. The baseline noise introduces a larger uncertainty in the calculation of the median value due to the integration of the noise. Therefore, while finding the most

probable values of velocity have only an uncertainty of ±500 m/s, the median values are closer to ±1,000 m/s to 1,500 m/s.

This method for analyzing the raw fluorescence traces is representative of the data analysis throughout this work. The median values of velocity and kinetic energy are reported, along with ranges for their distributions. Also, most probable values are used to show trends in the data, and to calculate the electric field using the $\vec{E} = -\nabla\phi$ relationship.

B. Centerline Measurements

Centerline measurements are presented for positions of $Z = -6$ mm inside the thruster channel to $Z = 40$ mm into the plume, as shown in Figure 8. For the positions inside the channel, only axial measurements are shown, while both axial and radial measurements are shown for positions in the plume.

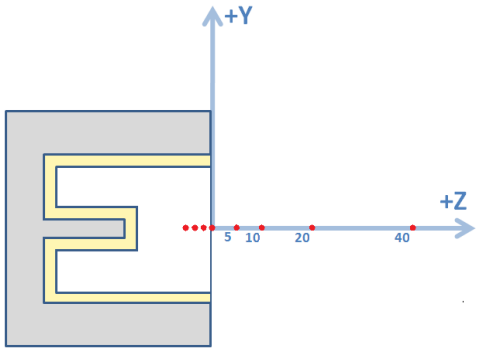

Figure 8. Location of data points for axial and radial LIF measurements along the centerline of the thruster.

1. *Ion Velocity Distributions*

Figure 9 shows the evolution of the ion velocity distributions for the CHT-30 at a) nominal and b) reduced magnetic field conditions. The red, dashed lines represent the radial distributions, while the blue solid lines represent the axial distributions.

In the axial direction, ion velocity distributions are shown both in the plume and at positions from $Z = -6$ mm to the exit plane within the thruster channel. For the nominal case, the distributions are relatively smooth and narrow, with 68% of the ions contained within less than a 4,000 m/s range (e.g. 2,900 m/s to 6,800 m/s for one standard deviation on each side of the median velocity at $Z = -2$ mm). For the reduced magnetic field condition, the axial ion velocity distributions are much broader inside the thruster, with less defined peaks giving ranges of approximately 5,000 m/s (e.g. 470 m/s to 5,500 m/s for one standard deviation from the median at $z = -2$ mm). Comparing the two, slight acceleration between Z = -6 mm and the exit plane can be seen in the nominal case, whereas it is less noticeable in the lower magnetic field case due to the broad distributions.

Referring back to Figure 3 which illustrates the cusped magnetic field profile inside a CHT – the magnetic field lines are believed to form equipotential surfaces, creating an electric field that has a significant axial component.[2] This causes a convergent ion flux[20] to keep ions away from the channel walls and accelerates the ions along the centerline. Therefore, it is intuitive that the nominal, higher magnetic field case, would have more noticeable acceleration and concentrated velocity distribution inside the channel due to better ion confinement along the centerline. Overall, however, the most probable axial velocities achieved by the nominal and reduced magnetic field cases are the same within the uncertainty of the measurements, at 6,500 m/s.

Outside the thruster channel, a significant portion of the axial ion acceleration is seen in the plume. For the nominal case, the ions achieve axial velocities between 16,000 m/s and 22,000 m/s at $Z = 40$ mm, with a relatively consistent acceleration from the exit plane through to the far field of the plume. For the reduced magnetic field case, the axial ion velocity distributions narrow and have a more pronounced peak as the ions progress further into the plume.

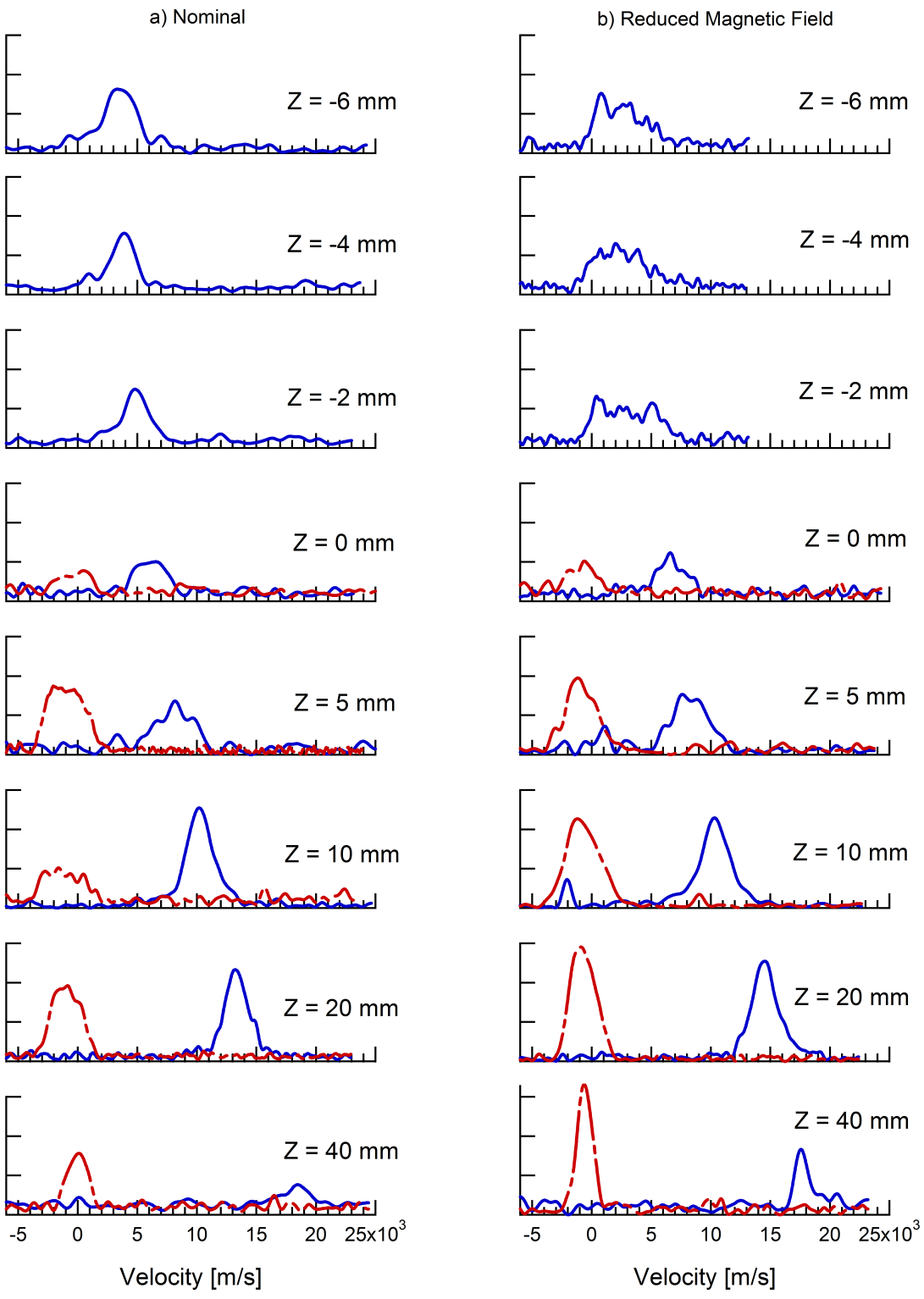

Figure 9. Centerline ion velocity distributions for the nominal and reduced magnetic field operating conditions. Red (– —) is the radial distribution, blue (—) is the axial distribution. The distributions are area normalized.

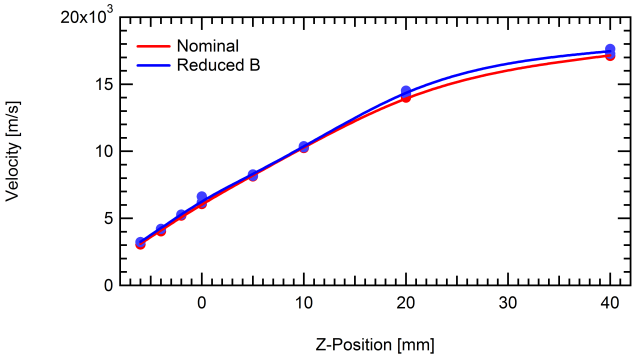

Figure 10. Most probable axial velocities along centerline of thruster plume for nominal and reduced magnetic field conditions.

Figure 10 depicts the most probable axial ion velocities along the centerline of the thruster from $Z = -6$ mm inside the thruster channel to $Z = 40$ mm into the plume. This figure shows that the reduced magnetic field case has a slightly higher most probable axial ion velocity from $Z = 10$ mm to $Z = 40$ mm, with the nominal case reaching 17,200 m/s and the reduced magnetic field case reaching 17,700 m/s at $Z = 40$ mm.

For both conditions, the radial velocity distribution remains relatively constant along the centerline of the thruster, centered near 0 m/s. Previous calculations show that the most probable radial velocities vary from zero by no more than 1,200 m/s.[1]

For both conditions, the radial ion velocities tend to have wider distributions at locations close to the exit plane of the thruster as compared to the points farther into the plume. This could be indicative of the strongly curved magnetic field profile seen in cusped-field thrusters that produces a wide distribution of velocity classes near the exit plane. This effect diminishes in strength farther downstream, due to the reduced influence of the radial component of electric field farther from the exit plane.

Alternatively, the field strength may be strong enough to produce Zeeman broadening. However, by comparing the two operating conditions, it is noticeable that the reduced magnetic field case tends to have wider radial ion velocity distributions, but sharper peaks in the axial velocity than the nominal case – indicating that while Zeeman broadening may be present, it is not the dominant broadening mechanism. Near the exit plane of the thruster, the wide radial distributions in the lower magnetic field case could be a function of the ions with slower axial velocities being pulled more effectively in the radial direction by the strong radial component of electric field. Similar to the axial velocity distributions, a stronger magnetic field seems to produce less variation in radial velocities.

2. Ion Kinetic Energy Distributions

Figure 11 shows the ion kinetic energy distributions at the centerline of the thruster channel for the nominal (red) and reduced magnetic field (blue) conditions. Previous studies on the CHT showed that the majority of the xenon propellant is ionized at the border of the annular and cylindrical region inside the CHT-30. The ion acceleration then occurs in the cylindrical region of the channel, along which the greatest potential drop occurs.[20] However, comparing the centerline kinetic energies achieved by the exit plane of the thruster channel to those achieved outside shows that a large portion of the axial acceleration actually occurs in the thruster plume, at positions further than $Z = 5$ mm.

Throughout the plume, the width of the kinetic energy distributions remains similar for both operating conditions. However, at $Z = 40$ mm, the distribution for the nominal condition becomes much wider than that of the reduced magnetic field case (i.e. the full-width at half maximum (FWHM) is 25 eV for the reduced magnetic field case, and 50 eV for the nominal case). The wings of the energy distributions, however, when measured by one standard deviation on either side of the median kinetic energy value give a range of 177 eV to 228 eV for the nominal case, and 191 eV to 270 eV for the reduced magnetic field case – a wider range of higher energy ions for the reduced magnetic field case.

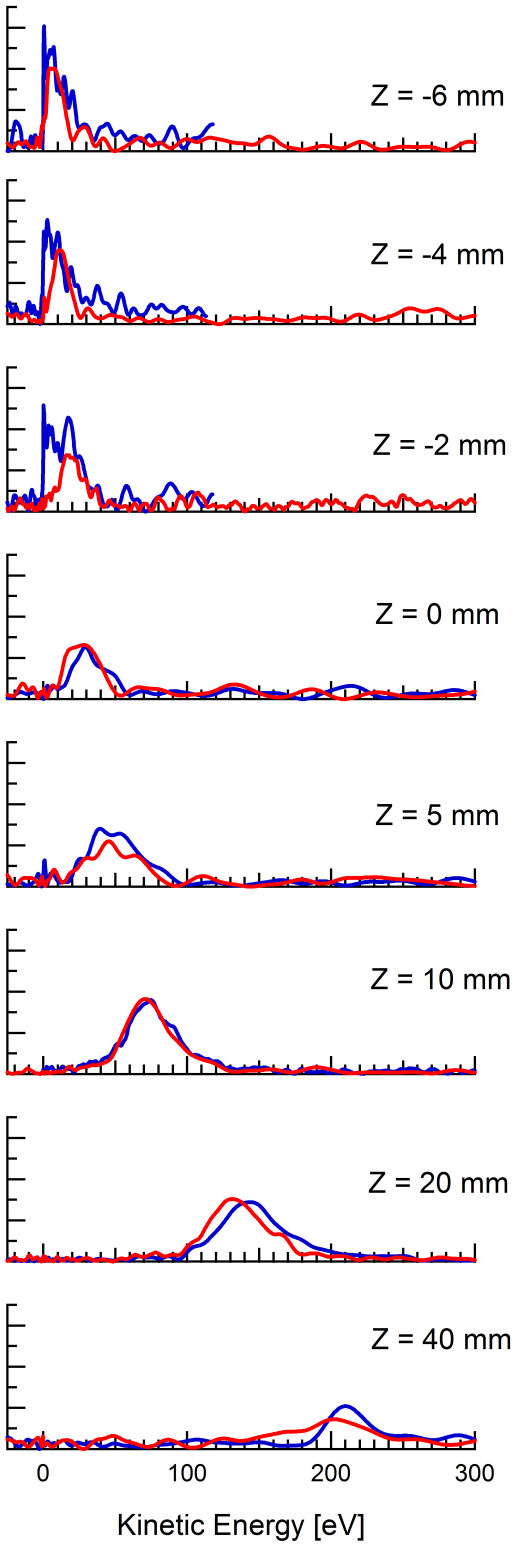

Figure 11. Centerline ion kinetic energy distributions for the nominal operating condition in red and reduced magnetic field operating condition in blue. The distributions are area normalized.

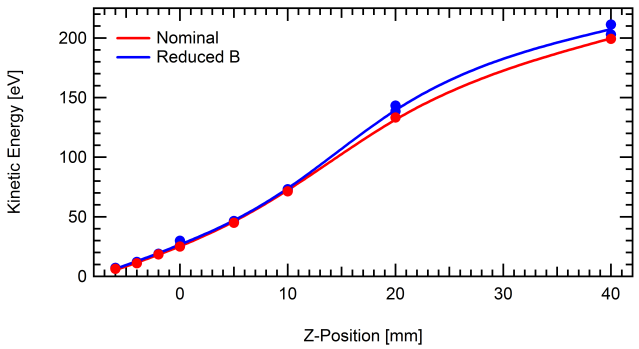

Figure 12. Most probable axial kinetic energies along centerline of plume for nominal and reduced magnetic field conditions.

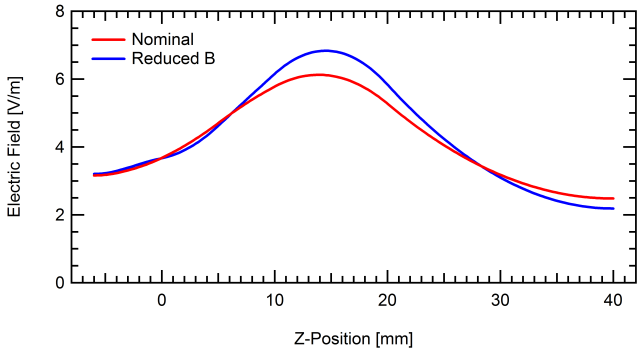

Figure 13. Centerline axial electric fields derived from most probable kinetic energies for nominal and reduced magnetic field conditions.

The reason the range over which the reduced magnetic field kinetic energies is wider in terms of percentage of ions is that while the peak in the kinetic energy distribution is sharper for this condition, the wings are much shallower, favoring the higher energy side of the distribution. The reduced magnetic field condition appears to accelerate the ions more effectively at locations farther into the plume.

Figure 12 shows the most probable axial kinetic energies along the centerline of the plume. The most probable value for both the nominal and reduced magnetic field kinetic energy is approximately 25 eV at the exit plane of the thruster, with an additional 175 eV to 188 eV gain in the plume. At a position 40 mm into the plume, this constitutes an energy of 200 eV for the nominal case and 213 eV for the reduced magnetic field case for an applied potential of 300 V. This confirms that the acceleration is primarily outside the thruster channel.

Figure 13 shows the axial electric field along the centerline of the thruster, derived from the most probable kinetic energy values. Comparing the electric fields makes the differences in acceleration seen in the velocity and kinetic energy distributions more clear. The reduced magnetic field case has a noticeably higher axial electric field around $Z = 10$ mm to 20 mm, allowing the ions to gain more energy in this region as compared to the nominal condition.

C. Centerline Measurements at High Background Pressure

The reduced magnetic field condition was also run with a higher chamber background pressure of 3.2×10^{-5} torr, for several positions throughout the plume. Figure 14 shows the velocity distributions in the radial and axial directions along the centerline of the thruster. As seen in the previous conditions, the radial velocity distributions remain relatively constant, centered around zero throughout the plume. For the axial direction, however, there is a large increase in velocity between $Z = 0$ mm and 5 mm, not seen in the lower pressure conditions. This is easily seen in Figure 15 which shows the most probable velocities along the centerline of the thruster.

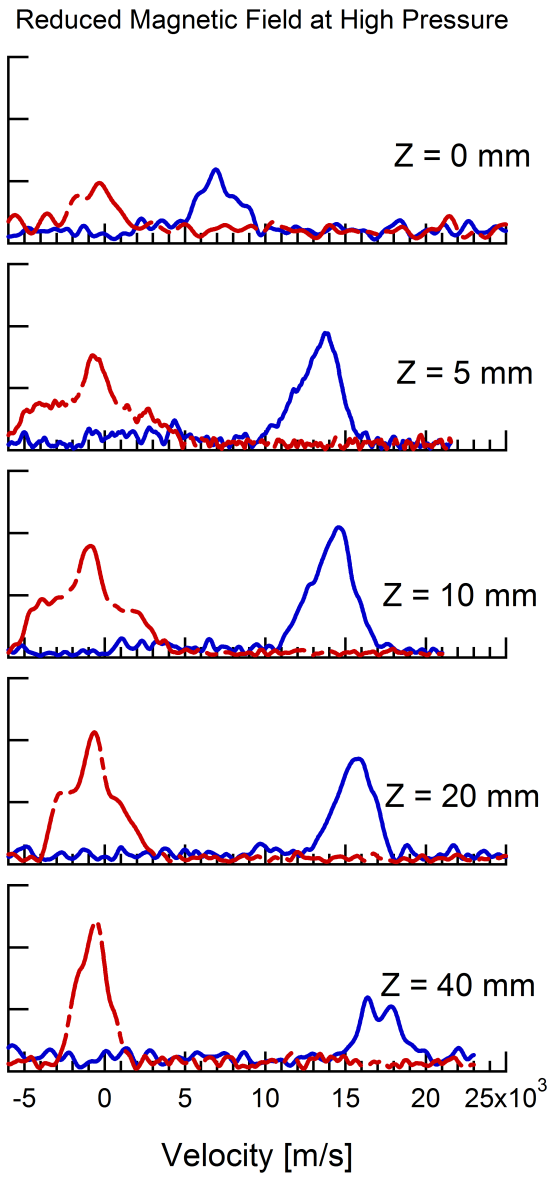

Figure 14. Effect of high pressure on reduced magnetic field condition velocity distributions. Red (– —) is the radial distribution, blue (—) is the axial distribution. The distributions are area normalized.

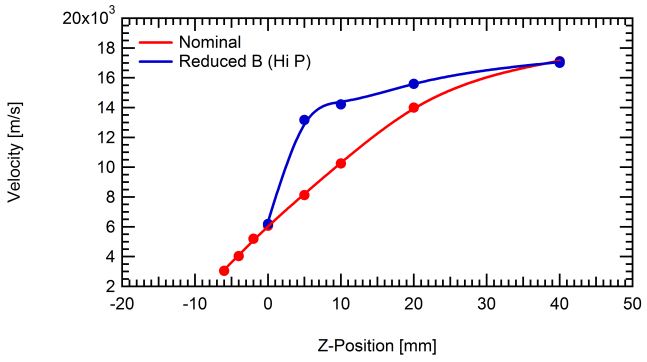

Figure 15. Most probable axial velocities along centerline of thruster plume for nominal and high pressure reduced magnetic field conditions.

Figure 16 shows the axial kinetic energy distributions for this higher pressure case, with the nominal condition also shown for comparison. It is evident that between $Z = 0$ mm and 5 mm, the gain in kinetic energy by far surpasses that seen in the nominal condition. But by $Z = 40$ mm, the axial ion kinetic energies become nearly the same.

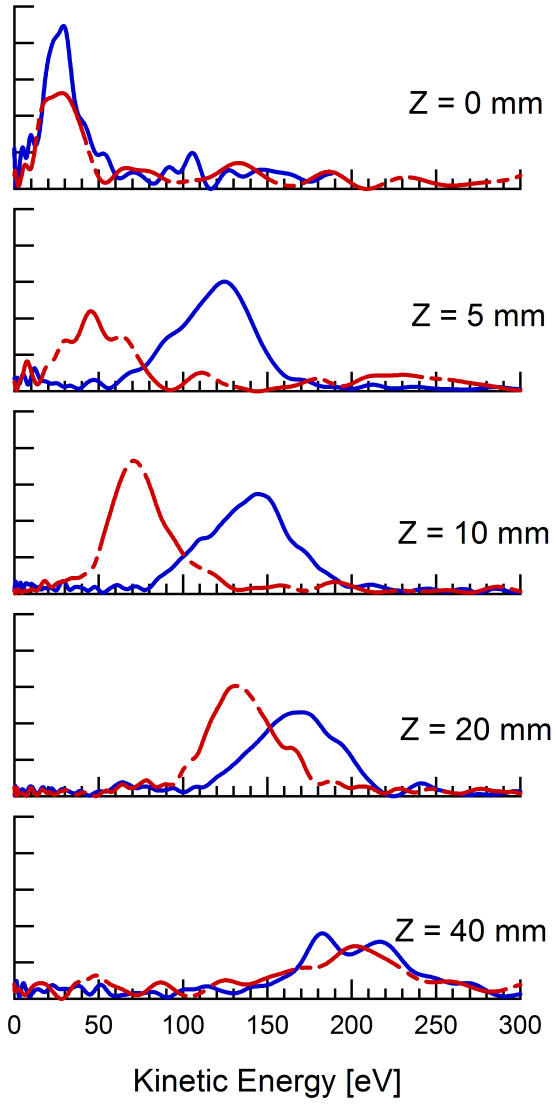

Figure 16. Effect of high pressure on reduced magnetic field condition kinetic energy distributiosn. Blue is the reduced magnetic field at high pressure condition, while red (– —) is the nominal condition, shown for reference. The distributions are area normalized.

This is summarized in Figure 17, which shows the most probable kinetic energies along the centerline of the thruster. For both the nominal and high pressure reduced magnetic field cases, the kinetic energy is around 25 eV at the exit plane of the thruster. The high pressure case gains nearly 100 eV of energy in the first 10 mm of the plume whereas the nominal case gains approximately 20 eV. By $Z = 40$ mm, the ion energies are once again very comparable with most probable values near 200 eV.

For both cases, the wings of the velocity distributions stretch between approximately 175 eV and 225 eV for 68% of the ions, showing that a good portion of the applied 300 V anode potential is used to accelerate the ions in the axial direction, but still less than in the reduced magnetic field case at lower pressure.

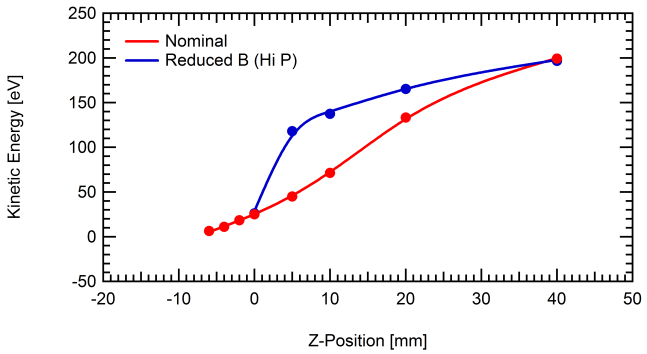

Figure 17. Most probable axial kinetic energies along centerline of thruster for nominal and high pressure reduced magnetic field conditions.

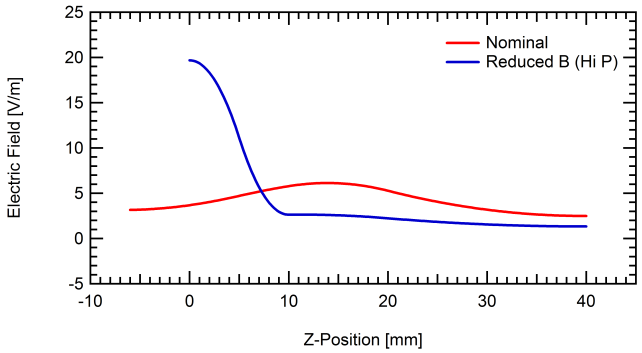

Figure 18. Centerline axial electric fields derived from most probable kinetic energies for nominal and high pressure reduced magnetic field conditions.

Figure 18 compares the electric field of the reduced magnetic field at high pressure condition to the nominal condition. This figure shows very distinctly that raising the background pressure in a vacuum chamber moves the acceleration region upstream towards the exit plane of the thruster. Previous work on a co-axial Hall thruster showed a similar effect[21] – increasing the background pressure changed the shape of the electric field and shifted the ion acceleration upstream towards the thruster exit plane.

D. Exit-plane Measurements

Exit plane measurements are presented for positions of $Y = 0$ mm to 14 mm along the face of the thruster channel at $Z = 0$ mm, as shown in Figure 19. Both radial and axial measurements are given at each point.

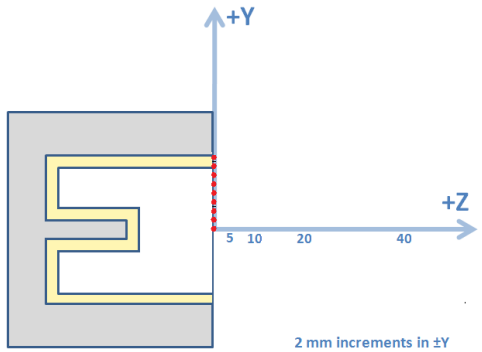

Figure 19. Location of measurement positions for axial and radial LIF measurements along the centerline.

1. *Ion Velocity Distributions*

Figure 21 shows the progression of ion velocity distributions across the exit plane of the thruster channel. Both the nominal and reduced magnetic field conditions behave similarly across the exit plane. The axial velocities slowly decrease across the width of the channel towards $Y = 14$ mm. The axial distributions broaden at positions away from the centerline, indicating a wider range of ion velocities, including a lower velocity tail in the distribution.

For example, the nominal condition at $Y = 0$ mm has a median axial velocity of 5,960 m/s, with wings spanning 3,160 m/s to 7,870 m/s for 68% of the ions. At $Y = 14$ mm, the median axial velocity is slower at 4,630 m/s, with a wider span of 1,850 m/s to 8,640 m/s. The reduced magnetic field case loses slightly less axial velocity, starting at 6,600 m/s at $Y = 0$ mm and decreasing to 5,860 m/s at the channel wall. For both cases, this could be reminiscent of the convergent ion flux inside the thruster channel previously described by Smirnov, et al.,[20] where the more energetic ions are kept away from channel walls.

Moving across the exit plane, the ions increase in radial velocity towards the channel wall. Starting at the centerline, the radial component of ion velocity is nearly zero for both operating conditions. But at a position of $Y = 14$ mm, the radial velocities become comparable in magnitude to the axial velocities. Figure 20 gives the most probable values, 4,360 m/s for the nominal condition (compared to 4,630 m/s in the axial direction) and 4,870 m/s for the reduced magnetic field condition (compared to 5,860 m/s in the axial direction). This high radial component of ion velocity at the exit plane is indicative of the large plume divergence half angle that is typical of cylindrical Hall thrusters, but is very different than traditional annular Hall thrusters where the exit plane axial component of velocity is much higher than the radial.[12]

Also of note in Figure 20 is that the most probable radial velocities at $Y = 0$ mm are negative values. Besides the ±500 m/s uncertainty, there are several contributing factors that may cause these velocities to be non-zero. These include the possibility that the centerline thruster is slightly misaligned, or more likely that the cathode being on one side of the thruster makes the plume slightly asymmetric.

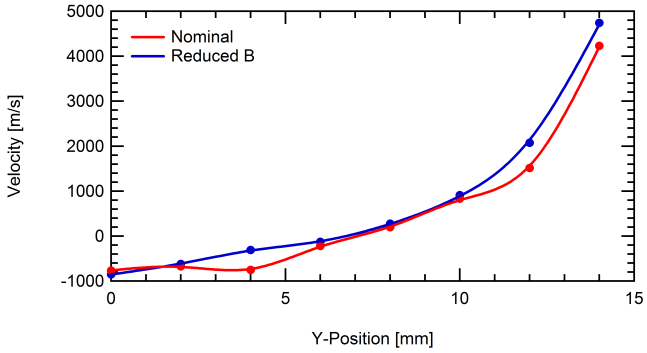

Figure 20. Most probable radial velocities along exit plane of thruster for nominal and reduced magnetic field conditions.

2. *Ion Kinetic Energy Distributions*

Figure 22 shows the radial kinetic energy distributions across the exit plane of the thruster. For both operating conditions, between positions of $Y = 0$ mm and $Y = 12$ mm, the peaks in the distributions are centered very close to 0 eV. Towards the channel wall, however, the tails of the distributions begin to stretch towards higher radial energies. The most probable radial kinetic energies are summarized in Figure 23. At $Y = 14$ mm, the most probable radial kinetic energy is 12 eV for the nominal case and 14 eV for the reduced magnetic field case. Adding these values to the nominal axial kinetic energies, 15 eV for the nominal case and 23 eV for the reduced magnetic field case at $Y = 14$ mm, shows that there is actually a gain in energy towards the channel wall at the exit plane. Both conditions start at approximately 25 eV at $Y = 0$ mm. The nominal condition increases to 26 eV at the channel wall, and the reduced magnetic field case increases to 37 eV. Overall, while there appears to be a convergent ion flux inside the thruster channel, the kinetic energy distributions at the exit plane indicate that the ions are very divergent just outside the channel.

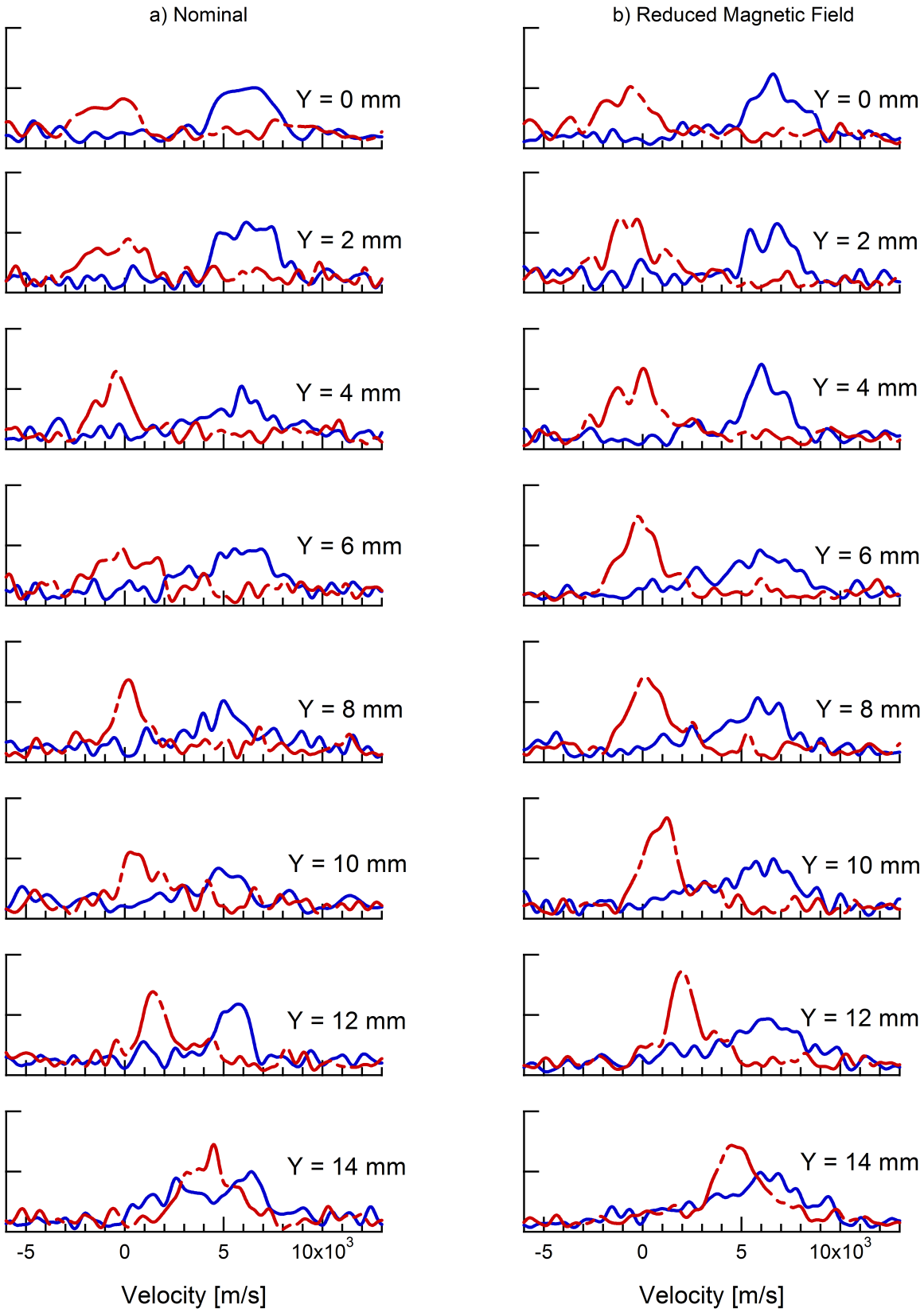

Figure 21. Exit plane ion velocity distributions for the nominal and reduced magnetic field operating conditions. Red (– —) is the radial distribution, blue (—) is the axial distribution. The distributions are area normalized.

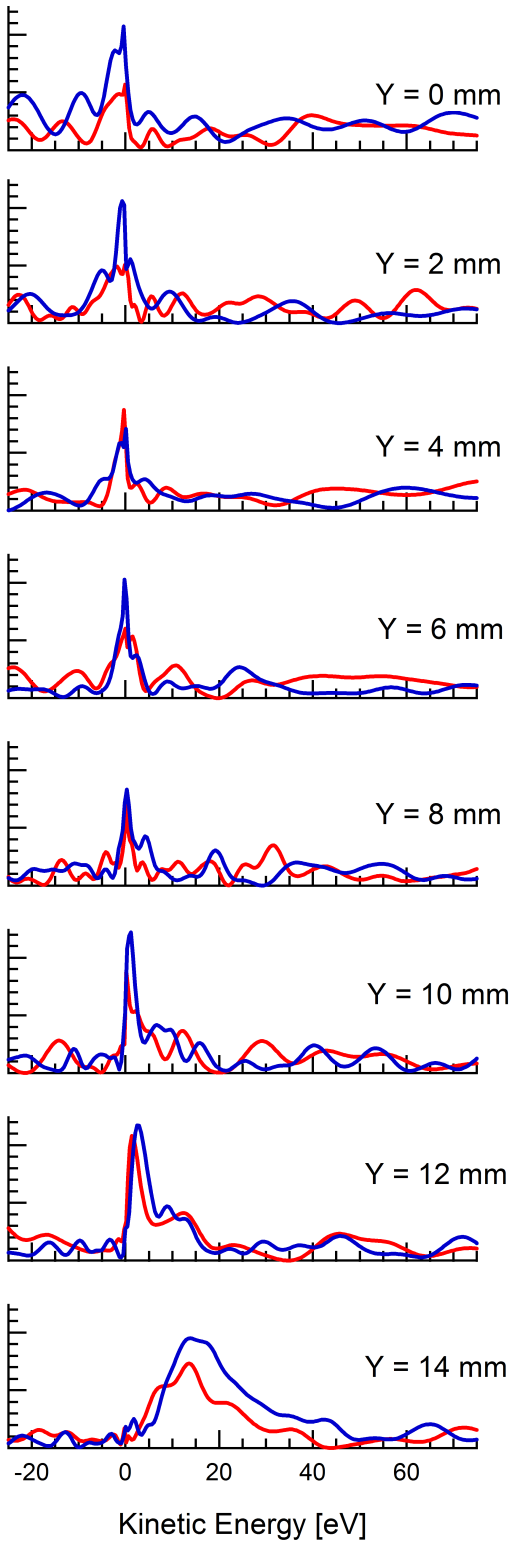

Figure 22. Most probable radial kinetic energy distributions along exit plane of thruster for nominal and reduced magnetic field conditions.

Figure 24 shows the radial electric field profile across the exit plane of the thruster, calculated from the most probable values of radial kinetic energy. Previous studies have shown the half angle of the plume to be as large as 60° to 80°, compared to traditional annular Hall thrusters which have plume divergence half angles of approximately 45° to 50°.[4] This increased divergence angle could be due to the radial component of the electric field in this region being stronger than that of a traditional annular Hall thruster.[2] This can be explained by the evolution of the magnetic field profile as it gets farther from the centerline of the channel. The resulting equipotential surfaces provide an electric field profile with a significant outward pointing radial component. From the exit plane outwards into the plume, all radial velocity components are therefore pointing away from the centerline. This plays a large role in the divergence of the plume, thereby reducing or eliminating the centerline ion flux seen inside the channel, resulting in a reduced mixing zone compared to annular Hall thrusters.

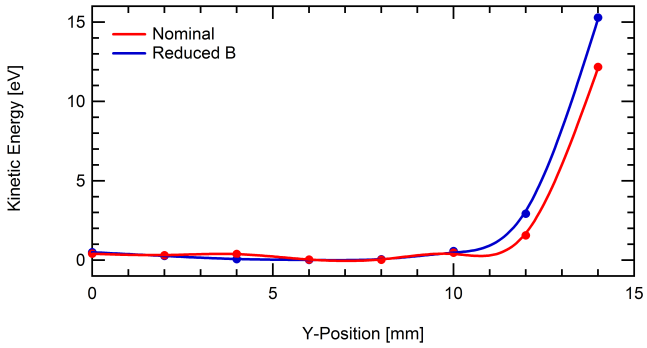

Figure 23. Most probable radial kinetic energies along exit plane of thruster for nominal and reduced magnetic field conditions.

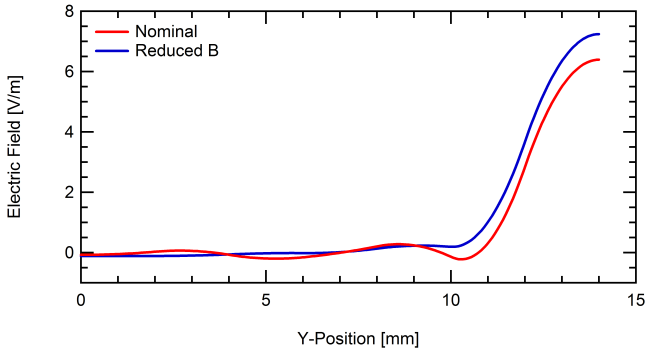

Figure 24. Exit plane radial electric fields derived from kinetic energies for nominal and reduced magnetic field conditions.

IV. Conclusions

Laser induced fluorescence was used to map the evolution of the ion velocity and kinetic energy distributions of the CHT-30 both inside the thruster channel and in the plume. A nominal operating condition was examined and compared to an reduced magnetic field case and the reduced magnetic field case at an elevated background pressure.

Inside the thruster channel, reduction of the magnetic field strength created wide velocity distributions with a larger portion of ions with slower axial velocities near the exit plane of the thruster. The nominal condition appeared to have more axial ion acceleration inside the channel, while the reduced magnetic field case had a greater acceleration in the plume, especially after $Z = 10$ mm. By 40 mm into the plume, the median axial ion kinetic energies were 200 eV for the nominal condition and 213 eV for the reduced magnetic field condition, with wings of the energy distributions approaching 270 eV, showing that a large portion of the applied 300 V anode potential went mostly into axially accelerating the ions.

Raising the background pressure had the effect of pushing the axial acceleration upstream towards the exit plane. This condition had the majority of its acceleration around $Z = 5$ mm. By $Z = 40$ mm, the velocities in the nominal condition caught up with the high pressure condition, resulting in similar distributions. The median axial kinetic energy for the high pressure case was approximately 200 eV at $Z = 40$ mm, with 68% of the ions having energies between 175 eV and 225 eV.

Looking at the distributions across the exit plane of the thruster, for both the nominal and reduced magnetic field operating conditions the radial component of ion velocity started near zero, then increased to be comparable in magnitude to the axial velocities near the channel wall. This agreed well with the large plume divergence angles seen in these type of thrusters, and indicated that the convergent ion flux seen inside the thruster channel disappears into a dispersed plume.

Along with an increased axial acceleration along the centerline of the plume, the increased radial velocity in the reduced magnetic field case implied that reducing the current to the electromagnets not only changed the magnetic field strength, but also the topology. Future work includes comparison of these CHT-30 results to LIF measurements on other types of cusped field thrusters, such as the MIT and Stanford Diverging Cusped Field Thrusters (DCFTs).[16,22]

V. Acknowledgments

The authors would like to thank D. L. O'Malley for his assistance in taking data, S. R. Gildea for his discussions about cusped field thrusters, and also Dr. C. W. Larson for sharing his knowledge of cylindrical Hall thrusters.

References

[1]MacDonald, N. A., Cappelli, M. A., and Hargus Jr., W. A., "Laser-Induced Fluorescence Velocity Measurements of a Low Power Cylindrical Hall Thruster," *Proceedings of the 31st International Electric Propulsion Conference*, 2009.

[2]Raitses, Y., Smirnov, A., and Fisch, N. J., "Cylindrical Hall Thrusters," *Proceedings of the 37th AIAA Plasmadynamics and Lasers Conference*, No. AIAA-2006-3245, American Institute of Aeronautics and Astronautics, June 2006.

[3]Hargus Jr., W. A. and Nakles, M. R., "Ion Velocity Measurements within the Acceleration Channel of Low-Power Hall Thruster," *IEEE Transactions on Plasma Science*, Vol. 36, No. 5, October 2008, pp. 1989–1997.

[4]Raitses, Y., Smirnov, A., and Fisch, N. J., "Enhanced performance of cylindrical Hall thrusters," *Applied Physics Letters*, Vol. 90, No. 221502, 2007.

[5]Hargus Jr., W. A. and Cappelli, M. A., "Laser-Induced Fluorescence Measurements of Velocity within a Hall Discharge," *Applied Physics B*, Vol. 72, No. 8, June 2001, pp. 961–969.

[6]Geisen, H., Krumpelmann, T., Neuschafer, D., and Ottinger, C., "Hyperfine Splitting Measurements on the 6265 Angstrom and 6507 Angstrom Lines of Seven Xe Isotopes by LIF on a Beam of Metastable Xe(3P0,3) Atoms," *Physics Letters A*, Vol. 130, No. 4-5, July 1988, pp. 299–309.

[7]Fischer, W., Huhnermann, H., Kromer, G., and Schafer, H. J., "Isotope Shifts in the Atomic Spectrum of Xenon and Nuclear Deformation Effects," *Z. Physik*, Vol. 270, No. 2, January 1974, pp. 113–120.

[8]Bronstrom, L., Kastberg, A., Lidberg, J., and Mannervik, S., "Hyperfine-structure Measurements in Xe II," *Physical Review A*, Vol. 53, No. 1, January 1996, pp. 109–112.

[9]Manzella, D. H., "Stationary Plasma Thruster Ion Velocity Distribution," *Proceedings of the 30th Joint Propulsion Conference and Exhibit*, No. AIAA-1994-3141, American Institute of Aeronautics and Astronautics, June 1994.

[10]Hansen, J. E. and Persson, W., "Revised Analysis of Singly Ionized Xenon, Xe II," *Physica Scripta*, , No. 4, 1987, pp. 602–643.

[11]Demtroeder, W., *Laser Spectroscopy: Basic Concepts and Instrumentation*, Springer-Verlag, 1996.

[12]Hargus Jr., W. A. and Charles, C. S., "Near Exit Plane Velocity Field of a 200-Watt Hall Thruster," *Journal of Propulsion and Power*, Vol. 24, No. 1, 2008, pp. 127–133.

[13]Miller, M. H. and Roig, R. A., "Transition Probabilities of Xe I and Xe II," *Physical Review A*, Vol. 8, No. 1, July 1973, pp. 480–486.

[14]Moore, C. E., *Atomic Energy Levels*, Vol. II, National Bureau of Standards, 1958.

[15]Smirnov, A., Raitses, Y., and Fisch, N. J., "Enhanced Ionization in the Cylindrical Hall Thruster," *Journal of Applied Physics*, Vol. 94, No. 2, 2003.

[16]Gildea, S. R., Batishchev, O., and Martinez-Sanchez, M., "Fully Kinetic Modeling of Divergent Cusped-Field Thrusters," *Proceedings of the 45nd Joint Propulsion Conference and Exhibit*, No. AIAA-2009-4814, American Institute of Aeronautics and Astronautics, August 2009.

[17]Gawron, D., Mazouffre, S., and Boniface, C., "A Fabry-Perot spectroscopy study on ion flow features in a Hall effect thruster," *Plasma Sources Science and Technology*, Vol. 15, 2006, pp. 757–764.

[18]Mazouffre, S., Gawron, D., Kulaev, V., and Sadehgi, N., "Xe+ Ion Transport in the Crossed-Field Discharge of a 5-kW-Class Hall Effect Thruster," *IEEE Transactions on Plasma Science*, Vol. 36, No. 5, October 2008, pp. 1967–1976.

[19]Hargus Jr., W. A. and Nakles, M. R., "Evolution of the Ion Velocity Distribution in the Near Field of the BHT-200-X3 Hall Thruster," *Proceedings of the 42nd Joint Propulsion Conference and Exhibit*, No. AIAA-2006-4991, American Institute of Aeronautics and Astronautics, July 2006.

[20]Smirnov, A., Raitses, Y., and Fisch, N. J., "Experimental and Theoretical Studies of Cylindrical Hall Thrusters," *Physics of Plasmas*, Vol. 14, No. 057106, 2007.

[21]Nakles, M. R. and Hargus Jr., W. A., "Background Pressure Effects on Internal and Near-field Ion Veloicty Distribution of the BHT-600 Hall Thruster," AIAA, Preprint (2009).

[22]Young, C. V., Smith, A. W., and Cappelli, M. A., "Preliminary Characterization of a Diverging Cusped Field (DCF) Thruster," *Proceedings of the 31st International Electric Propulsion Conference*, No. IEPC-2009-166, American Institute of Aeronautics and Astronautics, September 2009.